

Temperature Dependence of Dark Spot Diameters in GaN and AlGaN

Carsten Netzel,* Arne Knauer, Frank Brunner, Anna Mogilatenko, and Markus Weyers

Threading dislocations in c-plane (Al,Ga)N layers are surrounded by areas with reduced light generation efficiency, called “dark spots.” These areas are observable in luminescence measurements with spatial resolution in the sub-micrometer range. Dark spots reduce the internal quantum efficiency in single layers and light-emitting devices. In cathodoluminescence measurements, the diameter of dark spots (full width at half maximum [FWHM]) is observed to be 200–250 nm for GaN. It decreases by 30–60% for $\text{Al}_x\text{Ga}_{1-x}\text{N}$ with $x \approx 0.5$. Furthermore, the dark spot diameter increases with increasing temperature from 83 to 300 K in AlGaN, whereas it decreases in GaN. Emission energy mappings around dark spots become less smooth and show sharper features on sub-micrometer scales at low temperature for AlGaN and, on the contrary, at high temperature for GaN. It is concluded that charge carrier localization dominates the temperature dependence of dark spot diameters and of the emission energy distribution around threading dislocations in AlGaN, whereas the temperature-dependent excitation volume in cathodoluminescence and charge carrier diffusion limited by phonon scattering are the dominant effects in GaN. Consequently, with increasing temperature, nonradiative recombination related to threading dislocations extends to wider regions in AlGaN, whereas it becomes spatially limited in GaN.

dislocation core act as centers for fast non-radiative recombination and form local sinks for charge carrier density.^[5–10] The dark spots are formed by charge carrier diffusion to the carrier density sink and the resulting carrier density profile around threading dislocations.^[1,7,11–13] 2) Strain fields around the dominating threading edge dislocations generate bandgap variations and piezoelectric fields near the semiconductor surface in GaN.^[14–17] Excitons can dissociate in these piezoelectric fields, electrons and holes are separated, and the probability of radiative recombination is strongly reduced. The exciton dissociation should dominate the dark spot formation in GaN near the semiconductor surface, whereas charge carrier diffusion will prevail in the bulk.^[18]

Several studies have already examined characteristics of dark spots, especially their ability to reduce the light generation efficiency locally.^[3,6,7,11–15,17–23] However, in most of these studies, the binary semiconductor GaN was analyzed. Detailed studies of dark spot characteristics in AlGaN are

sparse and often restricted to the determination of their density.^[2,4,10,17,24]


Dark spots and the associated threading dislocations limit the quantum efficiency in c-plane III-nitride heterostructures.^[4,24–26] Accordingly, a reduction of the density of threading dislocations is key to improve internal quantum efficiency (IQE) of optoelectronic devices based on III-nitrides. The determination of dark spot densities, for example, by cathodoluminescence (CL) mappings, helps to achieve this goal, as it directly reflects the density of threading dislocations in the crystal.^[2,4,19,27,28] The diameter of dark spots, the area which is directly affected by reduced light generation efficiency, its temperature, and compositional dependence are not yet studied in detail for the ternary semiconductor AlGaN. Such studies could specify the degree of nonradiative losses provoked by threading dislocations in UV-B (ultraviolet B: 280–315 nm) and UV-C (ultraviolet C: 100–280 nm) LEDs more accurately.

In the current study, we evaluate the temperature-dependent diameter of dark spots in GaN and AlGaN bulk layers by CL. The layers are either undoped or Si doped to investigate possible screening effects by charge carriers on the dark spot diameter. We conduct hyperspectral mappings to collect spectrally resolved emission intensity and emission energy data on scales from nanometers to micrometers.

1. Introduction

Dark spots are observable in luminescence measurements with high spatial resolution of c-plane III-nitrides. They are caused by a reduced efficiency of light generation around threading dislocations. Dark spots are observed in bulk layers as well as in quantum well structures and heterostructures for light-emitting devices.^[1–4] The reduced light generation efficiency within dark spots in GaN seems to have at least two reasons. 1) Surface states at the dislocation core and possibly point defects near the

C. Netzel, A. Knauer, F. Brunner, A. Mogilatenko, M. Weyers
Ferdinand-Braun-Institut gGmbH
Leibniz-Institut für Höchstfrequenztechnik
Gustav-Kirchhoff-Strasse 4, Berlin 12489, Germany
E-mail: carsten.netzel@fbh-berlin.de

 The ORCID identification number(s) for the author(s) of this article can be found under <https://doi.org/10.1002/pssb.202100358>.

© 2021 The Authors. physica status solidi (b) basic solid state physics published by Wiley-VCH GmbH. This is an open access article under the terms of the Creative Commons Attribution License, which permits use, distribution and reproduction in any medium, provided the original work is properly cited.

DOI: 10.1002/pssb.202100358

2. Experimental Section

The studied c-plane GaN and AlGaIn layers were grown by metal-organic vapor phase epitaxy (MOVPE) on sapphire substrates in an AIX2600G3-HT reactor and a $6 \times 2''$ close-coupled showerhead reactor, respectively. Sample A was a 2.5 μm -thick non-intentionally doped (NID) GaN layer. The background silicon doping level was $[\text{Si}] < 10^{17} \text{ cm}^{-3}$. Sample B was a 3.7 μm -thick silicon-doped GaN layer ($[\text{Si}] = 4 \times 10^{18} \text{ cm}^{-3}$). Both GaN layers were grown after deposition of GaN nucleation and a 300 nm-thick GaN coalescence layer. Sample C was a 1600 nm-thick silicon-doped $\text{Al}_{0.47}\text{Ga}_{0.53}\text{N}$ layer ($[\text{Si}] = 1 \times 10^{19} \text{ cm}^{-3}$), grown on a sapphire/AlN template. Partial strain relaxation was realized by a 200 nm-thick AlN/GaN superlattice, a 600 nm-thick $\text{Al}_{0.73}\text{Ga}_{0.27}\text{N}$ layer, and a 1700 nm-thick compositionally graded $\text{Al}_{0.73 \rightarrow 0.47}\text{Ga}_{0.27 \rightarrow 0.53}\text{N}$ layer. The degree of relaxation of the analyzed top $\text{Al}_{0.47}\text{Ga}_{0.53}\text{N}$ layer with respect to the AlN template was determined to about 74% by X-ray diffraction analysis. Sample D was a 110 nm-thick NID $\text{Al}_{0.55}\text{Ga}_{0.45}\text{N}$ layer with a 100 nm-thick $\text{Al}_{0.96}\text{Ga}_{0.04}\text{N}$ blocking layer beneath. It was grown on a high-temperature-annealed (HTA) AlN/sapphire template with reduced threading dislocation density (TDD).^[29] A 900 nm-thick step-graded $\text{Al}_{0.93 \rightarrow 0.69}\text{Ga}_{0.07 \rightarrow 0.31}\text{N}$ layer was positioned between the template and the two top layers, leading to a degree of relaxation of 14% for the studied $\text{Al}_{0.55}\text{Ga}_{0.45}\text{N}$ layer. The TDD, determined by dark spot counting in CL, varied among the samples. It was $5 \times 10^8 \text{ cm}^{-2}$ for sample A and $8 \times 10^8 \text{ cm}^{-2}$ for sample B. It was higher for the AlGaIn layers on sapphire/AlN templates: $3 \times 10^9 \text{ cm}^{-2}$ for sample C and $1 \times 10^9 \text{ cm}^{-2}$ for sample D on the HTA template. The most relevant parameters for the analyzed top layers are shown in **Table 1**.

Temperature-dependent photoluminescence (PL) between $T = 10 \text{ K}$ and $T = 300 \text{ K}$ was used to investigate emission linewidth, degree of localization, and IQE for the four samples. A frequency-doubled argon-ion laser was used as an excitation source, providing an excitation power density of about 50 W cm^{-2} at 229 nm on a spot diameter of 70 μm . The PL emission was detected either with a radiometrically calibrated spectrometer for temperature-dependent measurements or with a 1 m monochromator, providing 20 pm spectral resolution, for measurements of the emission linewidths at $T = 10 \text{ K}$.

CL measurements were carried out in a Zeiss Ultra scanning electron microscope with a MONOCL4 detection unit from Gatan. The MONOCL4 unit was equipped with a 150 line cm^{-1} grating. Together with broad entrance and exit slits of 200 μm , the spectral resolution was about 3 nm. An acceleration voltage of 3 kV and a current of 700 pA were used for the 1 nm-wide scanning electron

Table 1. Aluminum content, silicon doping concentration, and TDD for the analyzed top layers in samples A–D.

(Al,Ga)N sample	Al content [%]	[Si] [cm^{-3}]	TDD [cm^{-2}]
A	0	$< 10^{17}$ (NID)	5×10^8
B	0	4×10^{18}	8×10^8
C	47	1×10^{19}	3×10^9
D	55	$< 10^{17}$ (NID)	1×10^9

beam on the sample surface to maintain an optimal spatial resolution together with sufficient luminescence intensity for data evaluation. Hyperspectral mappings in CL were measured with lateral spacings of 24 nm on the sample surfaces to ensure that the distance between adjacent excitation spots was smaller or similar to the expected diffusion length of charge carriers in the material ($\lambda_{\text{diff}}(T) = 30\text{--}200 \text{ nm}$ for GaN).^[18,30] Local emission intensity, peak emission energy, and emission linewidth (full width at half maximum/FWHM) distributions from the GaN and AlGaIn samples were deduced from the CL mappings. The CL measurements were carried out at stabilized sample temperatures of 83, 190, and 300 K at the same areas. The diameters of dark spots were determined from these intensity mappings by direct measurement of the distance between the dark spot center and a 50% intensity increase to nearby high-intensity areas (half width at half maximum/HWHM). Temperature-dependent hyperspectral mappings were acquired on several positions for each sample. This allowed to evaluate the widths of a larger number of dark spots for each sample, to increase statistics, and to take account of variations in dark spot diameters by dislocation types and possible local compositional variations in AlGaIn.

3. Results

3.1. IQE and Localization

Temperature-dependent PL measurements were carried out to provide data related to material homogeneity, degree of charge carrier localization, and IQE of the studied GaN and AlGaIn layers. The PL emission linewidth (FWHM) at $T = 10 \text{ K}$, determined with low excitation power density of $P = 50 \text{ W cm}^{-2}$ and with high spectral resolution, can be taken as a measure of the homogeneity of the bandgap. The low-temperature linewidth is small for the NID GaN sample A (FWHM = 2.4 meV), where the dominant donor-bound exciton transition defines the emission linewidth. The linewidth increases strongly for the ternary material AlGaIn or with silicon doping, so that differentiation between certain excitonic transitions near the bandgap is not possible anymore. The linewidths at $T = 10 \text{ K}$ are 8.7 meV for the Si-doped GaN (sample B), 83 meV for the Si-doped $\text{Al}_{0.47}\text{Ga}_{0.53}\text{N}$ (sample C), and 109 meV for the NID $\text{Al}_{0.55}\text{Ga}_{0.45}\text{N}$ (sample D). The high linewidths for the AlGaIn samples are mainly based on bandgap fluctuations caused by the statistical distribution of group-III atoms and the small exciton radius in AlGaIn.^[31,32] In addition, the AlGaIn composition can vary at certain growth features like growth islands,^[33] hillocks,^[34] or growth steps.^[35,36] The latter effects are rarely present in sample C, but add to the broader emission linewidth in sample D, where the studied AlGaIn layer is grown under a higher compressive strain.

Figure 1a shows the PL intensity plotted against the sample temperature for the four samples A–D. The stronger charge carrier localization in AlGaIn causes a stable PL intensity and reduced intensity losses in the low-temperature range $T = 10\text{--}100 \text{ K}$ for samples C and D. In the Si-doped samples B and C, the intensity decrease is less pronounced in the whole temperature range when compared with the NID GaN or AlGaIn samples A and D. Obviously, silicon doping is advantageous for a high IQE, too. Surely, there are further effects on PL intensity and its temperature

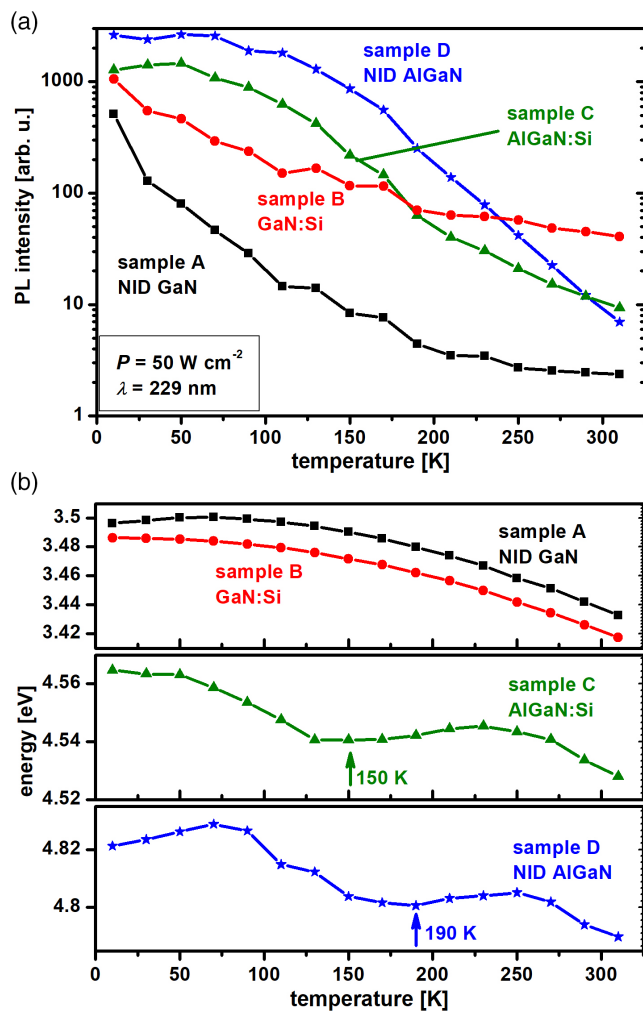


Figure 1. Temperature-dependent a) PL intensity and b) emission energy for samples A–D. The local minimum in the S-shape behavior of the emission energy is marked with an arrow for the AlGaN samples C and D.

dependence. Some of these effects shall just be mentioned but not be analyzed in detail. 1) Sample D has a high aluminum content barrier layer beneath the analyzed top layer preventing charge carrier diffusion into the bulk. In addition, sample D features a lower TDD than sample C. Both effects seem to increase the emission intensity, at least at $T = 10 \text{ K}$. 2) The ternary material AlGaN is more susceptible to increased incorporation of point defects, some of which might cause nonradiative recombination.^[37–40] This leads to stronger intensity losses around room temperature when charge carrier localization is overcome. 3) AlGaN layers in the medium range of composition may be subject to a temperature-dependent change of the occupation of their valence bands which can modify the degree of light polarization and the light outcoupling efficiency when temperature rises.^[41,42] This change in polarization results in changing slopes in the intensity versus temperature curves in Figure 1a, which are difficult to predict.

Figure 1b shows the PL emission energy plotted against temperature for samples A–D. The GaN samples feature a Varshni-like behavior, a monotonous decrease in emission energy with

increasing temperature based on the increase in the average lattice constants in the semiconductor crystal. The AlGaN samples C and D feature S-shape dependencies pointing to strong bandgap fluctuations and charge carrier localization. The local minimum of the emission energy, marked for the AlGaN samples by arrows in Figure 1b, is found at a slightly higher temperature for sample D. Together with the broader emission linewidth at $T = 10 \text{ K}$ this suggests a stronger degree of charge carrier localization and stronger bandgap variations for sample D when compared with sample C.^[43,44]

Overall, the presented data from temperature-dependent PL clearly prove charge carrier localization in the AlGaN samples C and D at low temperatures $T < 100 \text{ K}$ and delocalization around room temperature. The degree of localization is slightly higher for sample D. A relatively homogeneous bandgap and no charge carrier localization are present in the GaN samples A and B.

3.2. Hyperspectral CL Mappings

Figure 2a–f shows contour plots of the intensity, emission energy, and emission linewidth distributions on submicrometer scales for the NID GaN sample A and for the Si-doped AlGaN sample C. The data are deduced from hyperspectral CL mappings at $T = 83 \text{ K}$ and are shown exemplarily for mappings on further measurement positions and mappings for the other GaN and AlGaN samples B and D. Dark spots are shown in blue color in the intensity maps of Figure 1a,d. The density of dark spots and, accordingly, the density of threading dislocations are higher for the AlGaN sample C. This is caused by the nucleation process on sapphire with the formation of smaller nuclei in case of AlN nucleation and by a lower probability of dislocation annihilation in AlGaN when compared with GaN. The diameter of the dark spots is clearly smaller in the AlGaN sample. The diameter has a certain variance in the GaN sample as well as in the AlGaN sample. Yao et al. have shown that the contrast and the width of dark spots in GaN depend on the type of the threading dislocation in its center.^[22]

Figure 2b,e shows the emission energy distribution from the same areas. Depicted is the distribution of the peak energy derived from Gaussian fits to the local emission spectra. The peak emission energy varies by $\approx 4 \text{ meV}$ on the mapping for the GaN sample and by 20 meV for the AlGaN sample. In Figure 2c,f, the distribution of the emission linewidth in FWHM is presented, also derived by Gaussian fits to the local emission spectra. The emission linewidth of each local spectrum in the mapping is significantly broader than the peak energy variations in the same mapping. In case of AlGaN, thermal broadening at $T = 83 \text{ K}$ and the low spectral resolution in the CL setup can account only for a small part of the broad emission linewidth. Accordingly, strong bandgap fluctuations are present in the AlGaN sample on distances smaller than the obtained spatial resolution in the CL experiments. The spatial resolution is given by the excitation volume in the CL experiment, the lateral diffusion length, and in addition by local bandgap or field gradients which might cause charge carrier drift. In Figure 2d,e, dark spots and emission energy extrema with spacings of about $100\text{--}200 \text{ nm}$ are resolved for the AlGaN sample. Consequently, strong bandgap fluctuations in AlGaN can be

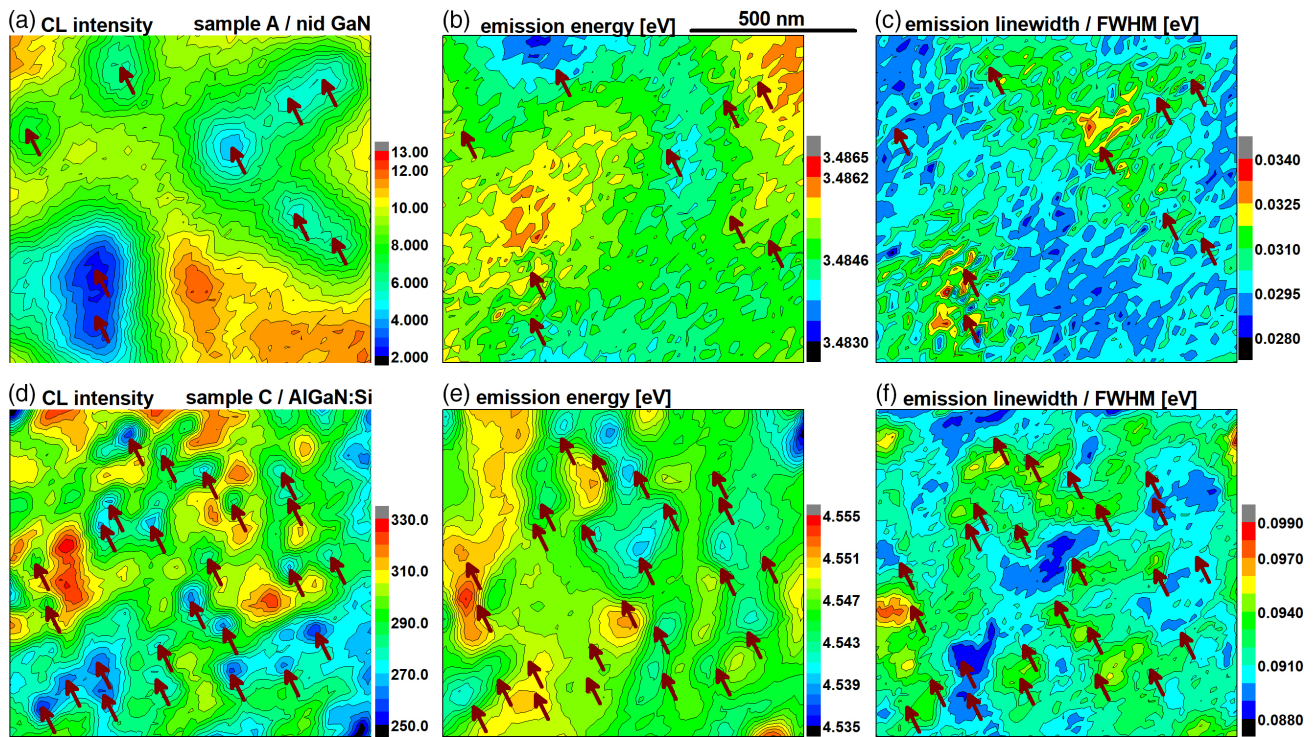


Figure 2. Evaluated hyperspectral CL mappings for a,b,c) the NID GaN sample A and d,e,f) the Si-doped AlGaIn sample C from CL measurements at $T = 83$ K. Emission intensity (a,d), peak energy (b,e), and linewidth maps (c,f) are shown from the same area. The arrows point to the center positions of dark spots, determined from the intensity map.

expected on even smaller distances. This circumstance will become important later on, in the discussion of the main findings.

The positions of dark spots are marked by arrows in Figure 2a–f. For GaN and for AlGaIn, the dark spot centers are not located at the positions where extrema of the emission energy can be found. Dark spots are generally located in areas with a high gradient in the emission energy. This correlation is caused by the strain profile, which is generated by the dominating threading edge dislocations and which leads to a potential dipole with highest bandgap gradient near the dislocation core.^[14–18,45,46] Spatially resolving these features is possible because the generation volume is smaller and the charge carrier diffusion lengths in the GaN and AlGaIn samples are shorter (see the study by Lähnemann et al.^[18]) than the dimensions of strain profiles and bandgap variations around dislocations. Nevertheless, according to their position in areas with high bandgap gradients, dark spots predominantly lie in regions with higher emission linewidth, shown in Figure 2c, f. Additional areas with bandgap extrema may be related to growth features, for example, growth step formation or island growth and the varying aluminum content based on these growth features in AlGaIn.^[33,35] Such growth features are not prominent in sample C. However, the underlying growth dynamics are still present and may cause additional emission energy extrema in Figure 2e.^[36]

3.3. T Dependence of Dark Spot Diameters

The temperature-dependent evolution of the intensity around dark spots in GaN and in AlGaIn is shown in Figure 3 by intensity

maps of the same area at sample temperatures of $T = 83$, 190, and 300 K. Results for the Si-doped samples B and C are shown as examples. The doped samples are chosen because of higher intensities and a better signal-to-noise ratio around room temperature. Concerning the dark spot characteristics, similar results are obtained for the NID samples A and D. Figure 3 shows that the dark spot diameter does not change strongly with temperature. However, a careful data evaluation reveals an important difference between GaN and AlGaIn: With increasing temperature, the diameter of the dark spots decreases in GaN, whereas it increases in AlGaIn. To prove this behavior more exactly we determined the widths of several dozen dark spots. The procedure is shown in the inset of Figure 4. We measured the HWHM of the intensity distribution around dark spots from several mappings similar to the examples shown in Figure 3. For the evaluation, cuts through the dark spot center with directions along the highest intensity gradients were chosen, directions toward adjacent dark spots were omitted. The resulting temperature-dependent widths of dark spots in samples A–D are shown in the diagrams of Figure 4. The scattering of the widths is strong because of varying types of threading dislocations,^[22] a generally inhomogeneous intensity level outside the dark spots, especially in case of AlGaIn, and the possible existence of unresolved dark spots when threading dislocations are close to each other.^[22] Data for sample D at $T = 190$ K are missing because of low CL intensity in combination with strong sample drift, limiting the integration time at this temperature. However, the observed trends are clear. The widths (HWHM) of dark spots in AlGaIn at $T = 83$ K, 52 nm for sample

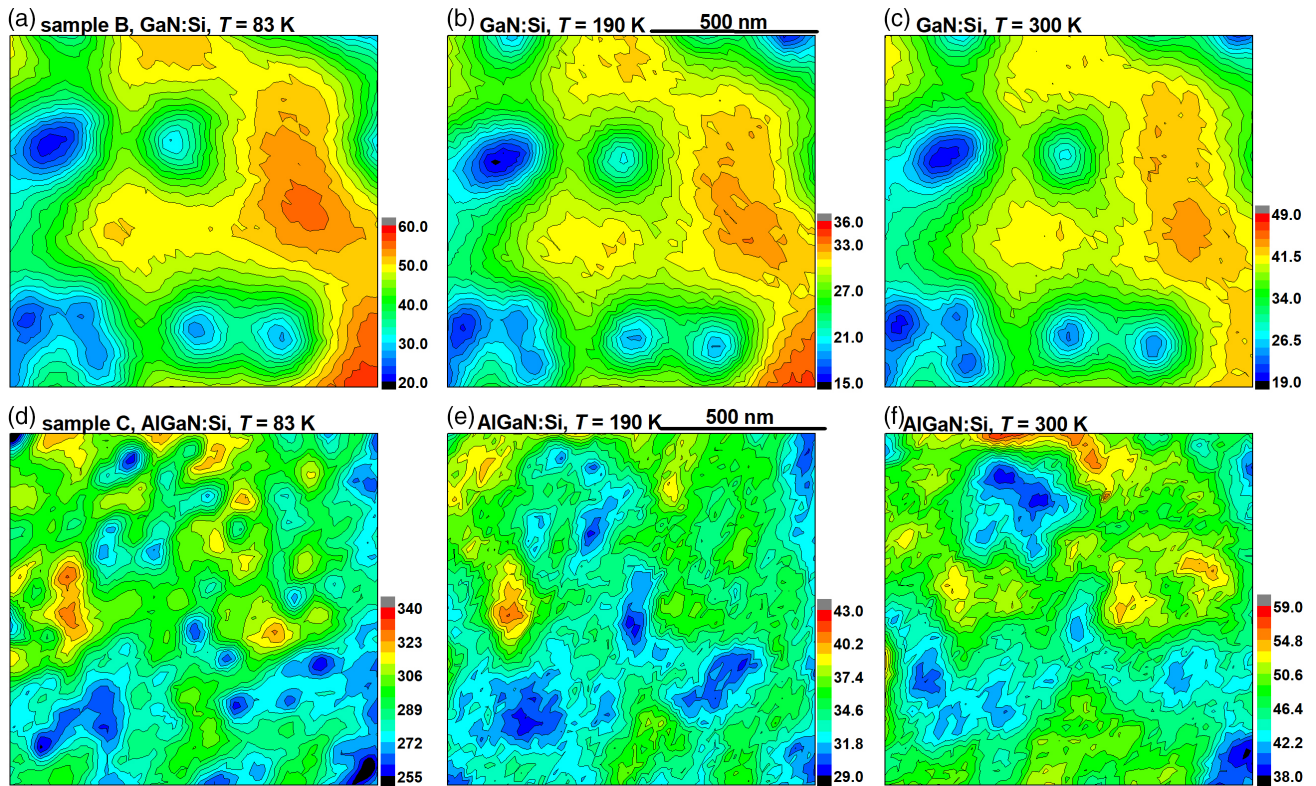


Figure 3. CL intensity maps with dark spots, measured with an acceleration voltage of 3 kV at differing sample temperatures for a,b,c) the Si-doped GaN sample B and d,e,f) the Si-doped AlGaN sample C.

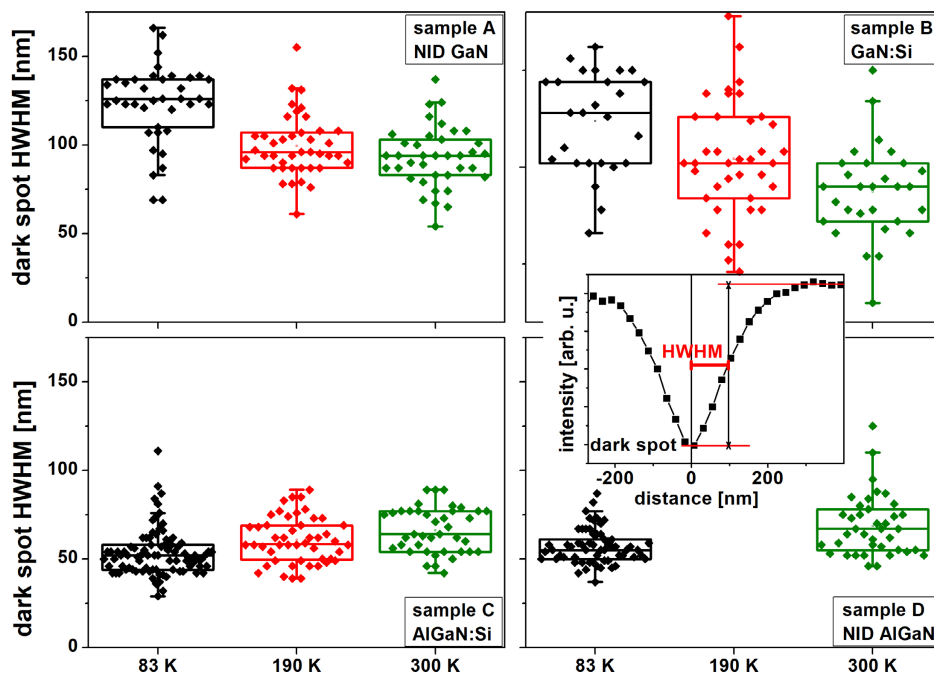


Figure 4. Dark spot widths for GaN and AlGaN samples A–D at different sample temperatures, derived from CL mappings with 3 kV acceleration voltage like in Figure 3. The procedure to determine the HWHM of the dark spots is shown in the inset.

C and 55 nm for sample D, are much smaller than in GaN, 126 nm for sample A and 114 nm for sample B. The diameter of dark spots for the GaN samples decreases with increasing temperature between $T = 83$ K and $T = 300$ K by 25% (sample A) or 17% (sample B). On the contrary, the diameter of dark spots increases with increasing temperature for the AlGaIn samples, by 23% (sample C) or 22% (sample D).

3.4. Emission Energy Distribution

The emission energy distribution around dark spots and threading dislocations can be used as a measure to evaluate whether the charge carrier diffusion increases or decreases by a change in sample temperature.^[18] Accordingly, temperature-dependent peak emission energy maps are shown in **Figure 5a–f**. Similar energy ranges of 7 meV (sample B) or 20 meV (sample C) are used in the mappings for each temperature. The variation in local emission energy clearly increases with increasing temperature for the GaN sample B, pointing to reduced charge carrier diffusion at elevated temperatures.^[18] Some of the charge carriers, excited by the electron beam, recombine near their excitation position. Diffusion to nearby areas with different bandgaps, especially to low-bandgap areas, is widely possible at low temperatures but becomes limited around room temperature because of increased phonon scattering. Accordingly, the energy distribution is smoother at low temperatures and contains more distinct extrema at higher temperatures. On the contrary, for the AlGaIn

sample C, the energy distribution shrinks to a narrower range at higher temperatures. Here, charge carrier diffusion seems to increase with increasing temperature between 83 and 300 K, leading to a more homogeneous emission energy map. Once more, we obtained similar results for the NID samples A and D.

4. Discussion

4.1. Comparison with Other III-Nitrides

The determined widths of dark spots in GaN and their temperature dependence (Figure 4) fit to recent observations by other groups.^[1,7,11–13,18] Below $T = 100$ K, widths of more than 100 nm (HWHM) are generally observed. The value decreases to <100 nm around room temperature. In case of a low acceleration voltage in CL measurements and surface-near excitation as in the current study, this behavior is mainly based on the temperature-dependent generation volume which shrinks at elevated temperatures because of more effective cooling of the generated hot carriers.^[18,47] The dark spots in AlGaIn under similar excitation conditions feature significantly smaller diameters of 50–70 nm HWHM than the dark spots in GaN (Figure 4). For other ternary III-nitride samples, for example, InGaIn quantum wells, the width of dark spots was found to be below 50 nm HWHM, also much smaller than that in bulk GaN.^[3] In addition, Bojarska-Ciešlińska et al. showed that the diameter of dark spots decreased with increasing indium content in the quantum

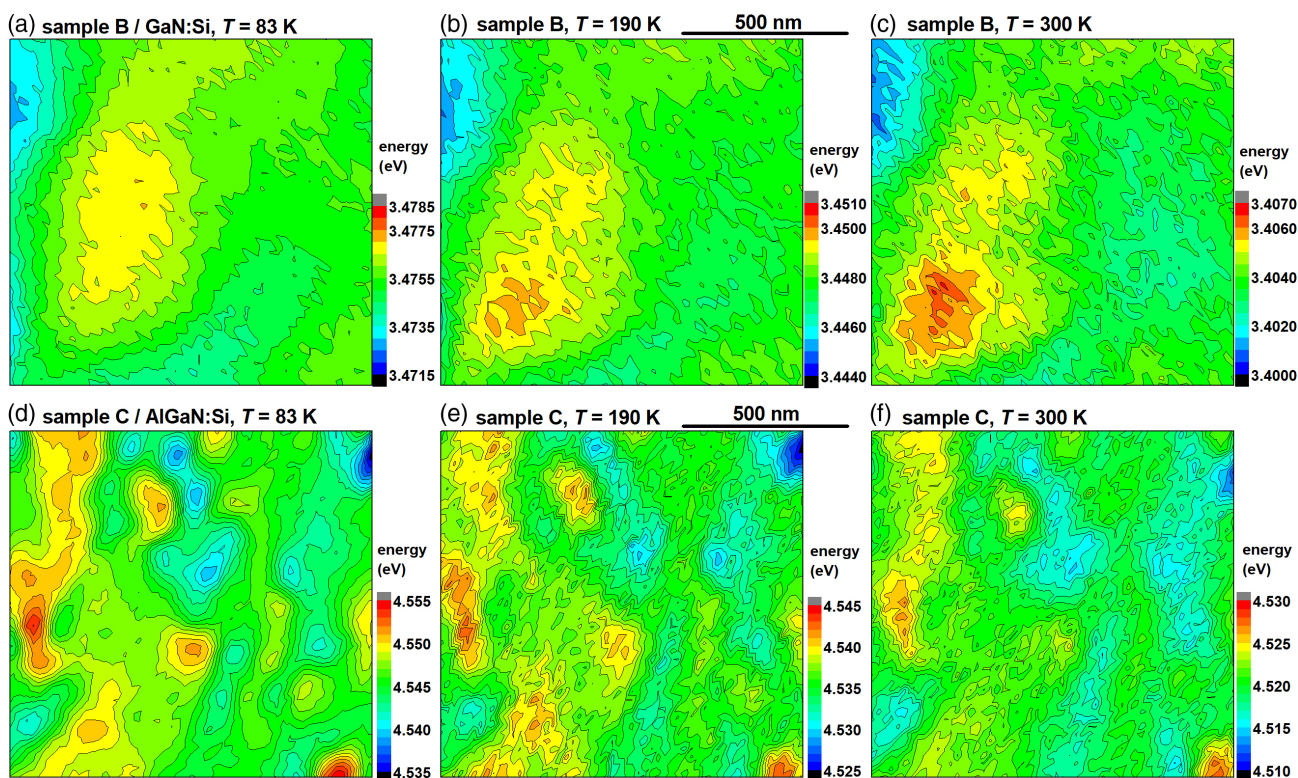


Figure 5. Peak emission energy mappings from CL with 3 kV acceleration voltage. The mappings are recorded at differing sample temperatures for a,b,c) the Si-doped GaN sample B and d,e,f) the Si-doped AlGaIn sample C.

wells.^[3] Ichikawa et al. studied dark spots in AlN and found widths of slightly less than 100 nm (HWHM) at $T = 80$ K for semipolar AlN and smaller dark spots in c-plane AlN.^[24] In both cases the dark spots became narrower at higher temperatures, similar to GaN. Overall, the dark spot diameter seems to decrease in ternary III-nitrides where charge carrier localization becomes prominent.

4.2. Localization Defining Dark Spot Diameters in AlGaN

Potential dipoles and c-plane piezoelectric fields around threading edge dislocations were identified as causes for the observation of dark spots in case of surface-near excitation in GaN.^[14,15,18] Excitons are dissociated and electrons and holes are separated in this potential landscape—what locally leads to reduced light generation. The same effect should be present in AlGaN, as piezoelectric polarization and strain relaxation in ternary nitrides behaves similar to the case of GaN. Following the calculations given by Kaganer et al.^[15] and considering GaN and AlN parameter sets for piezoelectric constants, elastic moduli, Burgers vectors, etc.^[48–50] as well as Vegard's law, the Coulomb potential and the piezoelectric field around the exit point of a threading edge dislocation at the crystal surface can be calculated. Potential and field are slightly higher for AlGaN when compared with GaN. Stronger piezoelectric fields around threading dislocations should increase the diameter of dark spots, as effective exciton dissociation is transferred to a wider radius around the dislocation core. However, the measured dark spot diameters shrink in AlGaN. Therefore, a change in strain relaxation and electric fields around threading edge dislocations, which is based on the additional aluminum content, should not be responsible for the observed smaller dark spot diameters in AlGaN.

Higher exciton binding energies in AlGaN and in InGaN quantum wells are also possible reasons for smaller dark spots.^[51,52] The strain-induced electric fields around threading edge dislocations which cause faster exciton dissociation are highest directly at the dislocation core and decrease with increasing distance proportional to r^{-1} .^[14,15] With a higher exciton binding energy, the radius defining relevant exciton dissociation would shift toward the dislocation core and the dark spot diameter would shrink. However, the dark spot diameter increases again for AlN,^[24] in spite of an even higher exciton binding energy than in AlGaN. So, the higher exciton binding energy in AlN may lead to smaller dark spots when the binary III-nitrides GaN and AlN are compared. For the ternary material AlGaN, another explanation is required to explain the smaller dark spot diameters.

Charge carrier localization in AlGaN can explain the observed small diameters of dark spots in AlGaN as well as their temperature-dependent extension. In GaN, values of a few hundred to less than hundred nanometers are observed for the charge carrier diffusion length, varying with temperature and excitation power.^[30,53] A shorter charge carrier diffusion length can be expected for AlGaN because of strong bandgap fluctuations. The smallest distance between spatially resolved emission energy extrema observed for the AlGaN sample C in Figure 2e is in the same range, about 100 nm. Furthermore, the locally measured emission spectra still feature linewidths of about 90 meV,

observable in the linewidth mapping in Figure 2f. The major part, about 50 meV, should be related to alloy broadening.^[31] When local bandgap variations of about 50 meV on distances of about 100 nm are considered, a lower limit for local bandgap gradients of about 10 kV cm^{-1} related to localization sites can be estimated. Pinos et al. and Saxena et al. even suggested bandgap gradients by compositional fluctuations on distances of less than 10 nm in AlGaN.^[33,54] Concerning this, local bandgap gradients related to localization in the order of 100 kV cm^{-1} can be expected. For comparison, the bandgap gradients based on strain around the exit point of threading edge dislocations should be $100\text{--}1000 \text{ kV cm}^{-1}$ in some nanometer-lateral distance to the dislocation core, but they decrease fast for higher distances.^[16,55] Piezoelectric fields near the sample surface feature values above 100 kV cm^{-1} in some nanometer distance to the dislocation core and decrease to 10 kV cm^{-1} in about 50 nm distance.^[15] Accordingly, local fields based on compositional variations in AlGaN are comparable with the bandgap gradients and piezoelectric fields based on strain around threading edge dislocations. In a certain distance to the dislocation core, local fields caused by compositional variations even exceed the strain-generated fields. This is shown in Figure 6. In some distance to the dislocation core, charge carriers can be trapped in localization sites in AlGaN and form excitons which can recombine radiatively, in spite of the superposition of a bandgap gradient or a piezoelectric field originating from the strain around the threading edge dislocation. In GaN, without localization, the excitons would drift along the bandgap gradient around the dislocation core or dissociate without the possibility to form again in localization sites. Consequently, the dark spot width, the limit, where radiative recombination becomes dominant, is smaller in AlGaN.

The dark spot width increases with increasing temperature in AlGaN. This is opposite to the observations in GaN and cannot be explained by a temperature-dependent change of the generation volume, like in the study by Jahn et al.^[47] With increasing temperature above 100 K, delocalization starts in the AlGaN samples, and charge carrier diffusion or hopping between localization sites sets in. The luminescence intensity starts to decrease because charge carriers reach nonradiative recombination centers more easily and the emission energy versus temperature curves converge toward a Varshni behavior (compare Figure 1). Consequently, charge carriers near threading edge dislocations react again to the bandgap gradients and piezoelectric fields. Dominant radiative recombination of excitons is gradually shifted toward areas far away from the dislocation core.

4.3. Dark Spots in Bulk

In the current study, the recombination around threading dislocations in GaN and AlGaN near the semiconductor surface was investigated and discussed so far. In the bulk, piezoelectric fields around threading edge dislocations are absent.^[14,16] In GaN bulk, the cores of threading edge dislocations were found to act as non-radiative recombination channels,^[18] and the area of low light generation efficiency around threading edge dislocations is given by charge carrier drift in the strain-induced bandgap gradient and the diffusion profile around the nonradiative dislocation core. The dark spot diameter should be reduced by phonon

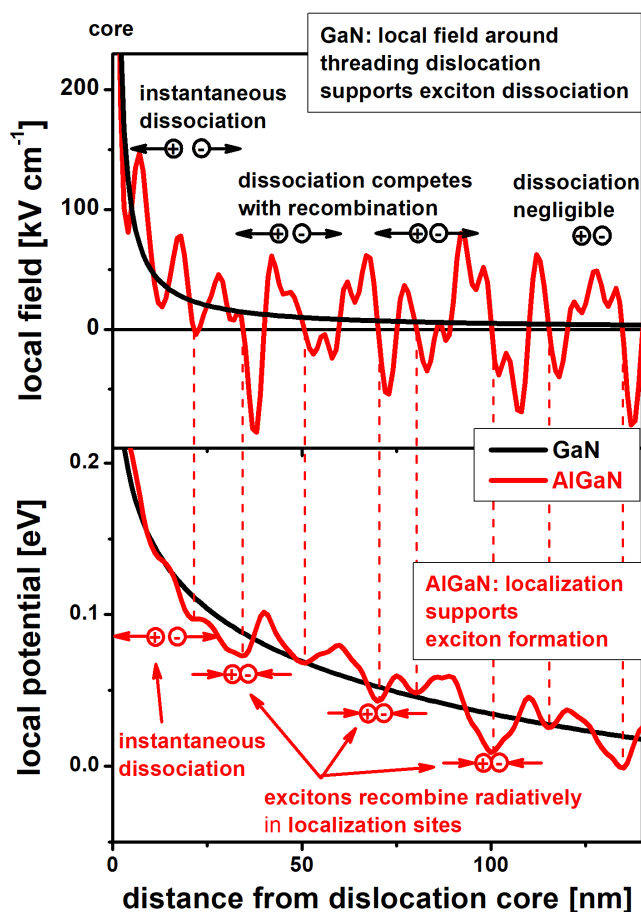


Figure 6. Illustration of the local field and the potential near the exit point of a threading edge dislocation in GaN (w/o charge carrier localization, black) and in AlGaIn (with localization, red). The noted values at x and y scales are not based on exact calculations; they should only indicate the expected dimensions of fields and potentials (compare values mentioned in the study by Kaganer et al.^[14]). Electron–hole pairs, excitons, are dissociated in a wide circle around edge dislocations in GaN and close to the dislocation core in AlGaIn. They can recombine radiatively in localization sites in some distance to the dislocation core in AlGaIn.

scattering at higher temperatures. From the previous discussion, it can be supposed for AlGaIn bulk that the areas with lower light generation efficiency around threading dislocations are also smaller than in GaN, because of limited charge carrier diffusivity and mobility based on localization. It can also be expected that these low-efficiency areas in AlGaIn bulk become broader with increasing temperature when charge carrier diffusion or hopping between localization sites sets in. However, a direct measurement of the temperature dependence of dark regions around threading dislocations in AlGaIn bulk would be a topic of future studies.

4.4. Impact on IQE

The impact of the dark areas around threading dislocations on the overall IQE varies among samples A–D. At $T = 83$ K, significant intensity losses of more than 25% by threading dislocations

are present on 50, 65, 50, and 20% of the total c-plane area for samples A, B, C, and D, respectively. So, for approximately half of the area in these samples, an estimation of an IQE near unity at low temperatures is not justified. The area with reduced intensity caused by threading dislocations decreases to 30 and 45% at room temperature for the GaN samples A and B. It increases to 75 and 30% for the AlGaIn samples C and D. The dark spot areas strongly contribute to reduced IQE, especially for samples A–C. Their temperature-dependent widening or narrowing will also affect the temperature-dependent intensity decrease measured, for example, by PL in Figure 1a. The relatively low area ratio of dark spots for sample D is caused by the low TDD of $1 \times 10^9 \text{ cm}^{-2}$ on the HTA template^[29] in combination with the reduced dark spot diameter in AlGaIn. For this and lower threading dislocation densities, areas without dark spots start to dominate over the dark spot areas. The spatially integrated intensity from the AlGaIn layer will come more from regions which are not affected by the presence of threading dislocations. The importance of point defects, formed far away from dislocations, will become more significant for nonradiative recombination in such regions. We observed temperature-dependent intensity decreases, which are equally strong within dark spots and in micrometer distance to dark spots. This finding confirms the importance of point defects as an additional limiting factor for the IQE in AlGaIn, which was recently discussed by Ichikawa et al.^[24]

4.5. Screening Effect by Doping

Finally, high silicon doping as applied in samples B and C is expected to cause a partial screening of piezoelectric fields or bandgap variations. Such a screening would result in a reduced diameter of dark spots in luminescence experiments with surface-near excitation. In fact, we observed slightly smaller dark spot diameters at $T = 83$ K in the doped samples B and C, when compared with the NID samples A and D. However, the effect is very small and not verifiable at each measured temperature in CL. At least, the doping effect on the dark spot widths is substantially smaller than the effect from localization caused by compositional disorder.

5. Conclusion

We have shown that dark spot diameters in c-plane AlGaIn are much smaller than in GaN under conditions of surface-near excitation in CL. Furthermore, the diameter of dark spots increases at higher temperatures in AlGaIn, whereas it decreases in GaN. Charge carrier localization, based on bandgap fluctuations on nanometer ranges, is suggested to be responsible for the differing characteristics of dark spot widths in AlGaIn when compared with GaN. As a consequence, areas with reduced light generation efficiency around threading dislocations in AlGaIn grow with increasing sample temperature and with decreasing compositional disorder, near the AlGaIn surface and in the bulk.

Acknowledgements

The authors thank C. Neumann and T. Petzke for their technical support during epitaxial growth. This work was partially funded by the

German Federal Ministry of Education and Research (BMBF) within the Advanced UV for Life consortium (UVPower, 03ZZ0134B).

Open access funding enabled and organized by Projekt DEAL.

Conflict of Interest

The authors declare no conflict of interest.

Data Availability Statement

Research data are not shared.

Keywords

AlGaN, cathodoluminescence, dark spots, internal quantum efficiency, threading dislocations

Received: July 23, 2021

Revised: August 17, 2021

Published online: September 6, 2021

-
- [1] D. Nakaji, V. Grillo, N. Yamamoto, T. Mukai, *J. Electron Microsc.* **2005**, 54, 223.
- [2] S. Kurai, K. Anai, H. Miyake, K. Hiramatsu, Y. Yamada, *J. Appl. Phys.* **2014**, 116, 235703.
- [3] A. Bojarska-Cieslińska, Ł. Marona, J. Smalc-Koziorowska, S. Grzanka, J. Weyher, D. Schiavon, P. Perlin, *Sci. Rep.* **2021**, 11, 21.
- [4] N. Susilo, E. Ziffer, S. Hagedorn, L. Cancellara, C. Netzel, N. Lobo Ploch, S. Wu, J. Rass, S. Walde, L. Sulmoni, M. Guttmann, T. Wernicke, M. Albrecht, M. Weyers, M. Kneissl, *Photonics Res.* **2020**, 8, 589.
- [5] K. Leung, A. F. Wright, E. B. Stechel, *Appl. Phys. Lett.* **1999**, 74, 2495.
- [6] S. J. Rosner, E. C. Carr, M. J. Ludowise, G. Girolami, H. I. Erikson, *Appl. Phys. Lett.* **1997**, 70, 420.
- [7] K. K. Sabelfeld, V. M. Kaganer, C. Pfüller, O. Brandt, *J. Phys. D: Appl. Phys.* **2017**, 50, 405101.
- [8] A. H. Cottrell, B. A. Bilby, *Proc. Phys. Soc. A* **1949**, 62, 49.
- [9] J. Elsner, R. Jones, M. I. Heggie, P. K. Sitch, M. Haugk, T. Frauenheim, S. Öberg, P. R. Briddon, *Phys. Rev. B* **1998**, 58, 12571.
- [10] G. Kusch, M. Nouf-Allahiani, F. Mehnke, C. Kuhn, P. R. Edwards, T. Wernicke, A. Knauer, V. Kueller, G. Naresh-Kumar, M. Weyers, M. Kneissl, C. Trager-Cowan, R. W. Martin, *Appl. Phys. Lett.* **2015**, 107, 072103.
- [11] T. Sugahara, H. Sato, M. Hao, Y. Naoi, S. Kurai, S. Tottori, K. Yamashita, K. Nishino, L. T. Romana, S. Sakai, *Jpn. J. Appl. Phys.* **1998**, 37, L398.
- [12] N. Pauc, M. R. Phillips, V. Aimez, D. Drouin, *Appl. Phys. Lett.* **2006**, 89, 161905.
- [13] N. Ino, N. Yamamoto, *Appl. Phys. Lett.* **2008**, 93, 232103.
- [14] V. M. Kaganer, J. Lähnemann, C. Pfüller, K. K. Sabelfeld, A. E. Kireeva, O. Brandt, *Phys. Rev. Appl.* **2019**, 12, 054038.
- [15] V. M. Kaganer, K. K. Sabelfeld, O. Brandt, *Appl. Phys. Lett.* **2018**, 112, 122101.
- [16] V. Taupin, C. Fressengeas, P. Ventura, M. Lebyodkin, V. Gornakov, *J. Appl. Phys.* **2014**, 115, 144902.
- [17] K. Forghani, L. Schade, U. T. Schwarz, F. Lipski, O. Klein, U. Kaiser, F. Scholz, *J. Appl. Phys.* **2012**, 112, 093102.
- [18] J. Lähnemann, V. M. Kaganer, K. K. Sabelfeld, A. E. Kireeva, U. Jahn, C. Chèze, R. Calarco, O. Brandt, (Preprint) arXiv:2009.14634, v1, unpublished, **2020**.
- [19] E. Meissner, S. Schweigard, J. Friedrich, T. Paskova, K. Udway, G. Leibiger, F. Habel, *J. Cryst. Growth* **2012**, 340, 78.
- [20] M. Albrecht, J. L. Weyher, B. Lucznik, I. Grzegory, S. Porowski, *Appl. Phys. Lett.* **2008**, 92, 231909.
- [21] W. Liu, J.-F. Carlin, N. Grandjean, B. Deveaud, G. Jacopina, *Appl. Phys. Lett.* **2016**, 109, 042101.
- [22] Y. Yao, Y. Sugawara, D. Yokoe, K. Sato, Y. Ishikawa, N. Okada, K. Tadatomo, M. Sudo, M. Kato, M. Miyoshi, T. Egawa, *CrystEngComm* **2020**, 22, 8299.
- [23] C. Shi, P. M. Asbeck, E. T. Yu, *Appl. Phys. Lett.* **1999**, 74, 573.
- [24] S. Ichikawa, M. Funato, Y. Kawakami, *Phys. Rev. Appl.* **2018**, 10, 064027.
- [25] M. Kneissl, T. Kolbe, C. Chua, V. Kueller, N. Lobo, J. Stellmach, A. Knauer, H. Rodriguez, S. Einfeldt, Z. Yang, N. M. Johnson, M. Weyers, *Semicond. Sci. Technol.* **2011**, 26, 014036.
- [26] K. Ban, J. Yamamoto, K. Takeda, K. Ide, M. Iwaya, T. Takeuchi, S. Kamiyama, I. Akasaki, H. Amano, *Appl. Phys. Express* **2011**, 4, 052101.
- [27] A. V. Govorkov, A. Y. Polyakov, T. G. Yugova, N. B. Smirnov, E. A. Petrova, M. V. Mezhenyi, A. V. Markov, I.-H. Lee, S. J. Pearton, *J. Surf. Invest.* **2007**, 1, 380.
- [28] E. D. Le Boulbar, J. Priesol, M. Nouf-Allahiani, G. Naresh-Kumar, S. Fox, C. Trager-Cowan, A. Šatka, D. W. E. Allsopp, P. A. Shields, *J. Cryst. Growth* **2017**, 466, 30.
- [29] S. Hagedorn, S. Walde, A. Knauer, N. Susilo, D. Pacak, L. Cancellara, C. Netzel, A. Mogilatenko, C. Hartmann, T. Wernicke, M. Kneissl, M. Weyers, *Phys. Status Solidi A* **2020**, 217, 1901022.
- [30] O. Brandt, V. M. Kaganer, J. Lähnemann, T. Flissikowski, C. Pfüller, K. K. Sabelfeld, A. E. Kireeva, C. Chèze, R. Calarco, H. T. Grah, U. Jahn, (Preprint) arXiv:2009.13983, v2, unpublished, **2020**.
- [31] S. Kurai, H. Miyake, K. Hiramatsu, Y. Yamada, *J. Appl. Phys.* **2016**, 119, 025707.
- [32] G. Coli, K. K. Bajaj, J. Li, J. Y. Lin, H. X. Jiang, *Appl. Phys. Lett.* **2001**, 78, 1829.
- [33] A. Pinos, V. Liulia, S. Marcinkevicius, J. Yang, R. Gaska, M. S. Shur, *J. Appl. Phys.* **2011**, 109, 113516.
- [34] S. Kurai, F. Ushijima, H. Miyake, K. Hiramatsu, Y. Yamada, *J. Appl. Phys.* **2014**, 115, 053509.
- [35] U. Zeimer, V. Kueller, A. Knauer, A. Mogilatenko, M. Weyers, M. Kneissl, *J. Cryst. Growth* **2013**, 377, 32.
- [36] U. Zeimer, J. Jeschke, A. Mogilatenko, A. Knauer, V. Kueller, V. Hoffmann, C. Kuhn, T. Simoneit, M. Martens, T. Wernicke, M. Kneissl, M. Weyers, *Semicond. Sci. Technol.* **2015**, 30, 114008.
- [37] T. A. Henry, A. Armstrong, A. A. Allerman, M. H. Crawford, *Appl. Phys. Lett.* **2012**, 100, 043509.
- [38] A. M. Armstrong, A. A. Allerman, *Appl. Phys. Lett.* **2017**, 111, 042103.
- [39] H. W. Jang, M.-K. Lee, H.-J. Shin, J.-L. Lee, *Phys. Status Solidi C* **2003**, 0, 2456.
- [40] S. F. Chichibu, A. Uedono, K. Kojima, H. Ikeda, K. Fujito, S. Takashima, M. Edo, K. Ueno, S. Ishibashi, *J. Appl. Phys.* **2018**, 123, 161413.
- [41] K. B. Nam, J. Li, M. L. Nakarmi, J. Y. Lin, H. X. Jiang, *Appl. Phys. Lett.* **2004**, 84, 5264.
- [42] C. Netzel, A. Knauer, M. Weyers, *Appl. Phys. Lett.* **2012**, 101, 242102.
- [43] R. Pecharrroman-Gallego, R. W. Martin, I. M. Watson, *J. Phys. D: Appl. Phys.* **2004**, 37, 2954.
- [44] C. Netzel, C. Mauder, T. Wernicke, B. Reuters, H. Kalisch, M. Heuken, A. Vescan, M. Weyers, M. Kneissl, *Semicond. Sci. Technol.* **2011**, 26, 105017.
- [45] N. Gmeinwieser, P. Gottfriedsen, U. T. Schwarz, W. Wegscheider, R. Clos, A. Krtschil, A. Krost, A. Weimar, G. Brüderl, A. Lell, V. Härle, *J. Appl. Phys.* **2005**, 98, 116102.
- [46] N. Gmeinwieser, U. T. Schwarz, *Phys. Rev. B* **2007**, 75, 245213.

- [47] U. Jahn, V. M. Kaganer, K. K. Sabelfeld, A. E. Kireeva, J. Lähnemann, C. Pfüller, C. Chêze, K. Biermann, R. Calarco, O. Brandt, (Preprint arXiv:2002.08713, v3, unpublished, **2020**.
- [48] J. Pal, G. Tse, V. Haxha, M. A. Migliorato, S. Tomić, *Phys. Rev. B* **2011**, *84*, 085211.
- [49] A. E. Romanov, T. J. Baker, S. Nakamura, J. S. Speck, ERATO/JST UCSB Group, *J. Appl. Phys.* **2006**, *100*, 023522.
- [50] I. Vurgaftman, J. R. Meyer, *J. Appl. Phys.* **2003**, *94*, 3675.
- [51] R. Ishii, M. Funato, Y. Kawakami, *Jpn. J. Appl. Phys.* **2014**, *53*, 091001.
- [52] A. Hangleiter, D. Fuhrmann, M. Grewe, F. Hitzel, G. Klewer, S. Lahmann, C. Netzel, N. Riedel, U. Rossow, *Phys. Status Solidi A* **2004**, *201*, 2808.
- [53] C. Netzel, V. Hoffmann, J. W. Tomm, F. Mahler, S. Einfeldt, M. Weyers, *Phys. Status Solidi B* **2020**, *257*, 2000016.
- [54] T. Saxena, S. Nargelas, J. Mickevičius, O. Kravcov, G. Tamulaitis, M. Shur, M. Shatalov, J. Yang, R. Gaska, *J. Appl. Phys.* **2015**, *118*, 085705.
- [55] D. Cherns, C. G. Jiao, H. Mokhtari, J. Cai, F. A. Ponce, *Phys. Status Solidi B* **2002**, *234*, 924.